Silica scaling in forward osmosis: From solution to membrane interface

Xie, Ming and Gray, Stephen (2017) Silica scaling in forward osmosis: From solution to membrane interface. Water Research, 108. 232 - 239. ISSN 0043-1354

Silica Scaling in Forward Osmosis: from Solution to Membrane Interface

Water Research

Revised: 5 August, 2016

Ming Xie [1*] and Stephen R. Gray [1]

[1] Institute for Sustainability and Innovation, College of Engineering and Science, Victoria University, PO Box 14428, Melbourne, Victoria 8001, Australia

[*]Corresponding author. E-mail: ming.xie@vu.edu.au

ABSTRACT

Membrane silica scaling hinders sustainable water production. Understanding silica scaling mechanisms provides options for better membrane process management. In this study, we elucidated silica scaling mechanisms on an asymmetric cellulose triacetate (CTA) membrane and polyamide thin-film composite (TFC) membrane. Scaling filtration showed that TFC membrane was subjected to more severe water flux decline in comparison with the CTA membrane, together with different scaling layer morphology. To elucidate the silica scaling mechanisms, silica species in the aqueous solution were characterised by mass spectrometry as well as light scattering. Key thermodynamic parameters of silica surface nucleation on the CTA and TFC membranes were estimated to compare the surface nucleation energy barrier. In addition, high resolution X-ray photoelectron spectroscopy resolved the chemical origin of the silica-membrane interaction via identifying the specific silicon bonds. These results strongly support that silica scaling in the CTA membrane was driven by the aggregation of mono-silicic acid into large silica aggregates, followed by the deposition from bulk solution onto the membrane surface; by contrast, silica polymerised on the TFC membrane surface where mono-silicic acid interacted with TFC membrane surface, which was followed by silica surface polymerisation.

Keywords: forward osmosis; silica scaling; cellulose triacetate; polyamide; silica aggregation; silica polymerisation

1. Introduction

Membrane-based water purification processes have played a crucial role in mitigating water scarcity worldwide (Elimelech and Phillip 2011, Shannon et al. 2008). One promising osmosis-driven membrane process, forward osmosis (FO) could potentially find a wide range of applications in water and wastewater treatment, particularly of challenging and difficult to treat wastewaters (Shaffer et al. 2015, Xie et al. 2016a). This capacity was mainly due to less detrimental and more reversible FO fouling in comparison with pressure-driven membrane process, such as and reverse osmosis (RO) (Lee et al. 2010, Mi and Elimelech 2010, Xie et al. 2015a, Xie et al. 2015b, Zou et al. 2011). Consequently, there have been several successful demonstrations of FO for the treatment of wastewaters with high fouling propensity with no or limited pretreatment, such as, anaerobic digester concentrate (Holloway et al. 2007, Xie et al. 2014), activated sludge solution (Achilli et al. 2009, Cornelissen et al. 2008), and municipal wastewater (Cath et al. 2005, Valladares Linares et al. 2011, Xie et al. 2013).

Silica, abudant in brackish groundwater, constrained water recovery and production in membrane filtration due to scaling (Milne et al. 2014). Previous knowledge from RO desalination showed that silica scaling was complicated due to the nature of silica chemistry, and was highly dependent on the opreating condition. Various silica scaling morphology was revealed on RO membranes ranging from patches of semi-transparent deposits (Den and Wang 2008) to opaque, milky to white gel (Aramaki et al. 2005), which indicated the complexity of silica scaling mechanisms. Although previous research efforts were made to gain a better understanding of silica scaling mechanisms and to develop scaling control strategies, silica scaling remains a major unsolved problem facing membrane desalination units.

Silica scaling was profiled in FO using silica colloidal particles as well as reactive silica. For instance, Boo et al. (2012) demonstrated severe silica colloidal scaling on FO membrane under elevated reverse salt diffusion. Reactive silica in seawater was attributed to the silica polymerisation on FO membrane surface, which was further aggravated by other natural organic compounds (Li et al. 2012). Silica scaling mechanisms were proposed by Mi and Elimelech (2013) following adhesion force measurement, where the adhesion force between polyamide thin-film composite (TFC) membrane was stronger than cellulose triacetate (CTA) membrane. However, this indirect approach cannot accurately reflect the silica scaling mechanisms in the filtration of aqueous solution as well as at the silica-membrane interface. In addition, the underlying chemical origin of silica membrane scaling remains unclear.

In this study, we investigated reactive silica scaling in FO using TFC and CTA membranes. Silica scaling behaviours – water flux decline and scaling layer morphology – were demonstrated. Silica scaling mechanisms were elucidated by characterising silica species in the aqueous solution, and thermodynamic parameters and chemical state of silicon bonds during silica-membrane interaction. Mass spectrometry and light scattering were used to characterise size and structure of silica species in the aqueous solution during silica scaling. Key parameters of silica surface nucleation were estimated using a series of silica filtration experiments. High resolution X-ray photoelectron spectroscopy was used to resolve the chemical origin of the silica-membrane interaction by identifying the specific silicon bonds.

2. Materials and methods

2.1. FO membranes and silica chemistry

An asymmetric cellulose triacetate (CTA) and a polyamide thin-film composite (TFC) forward osmosis (FO) membrane were employed in this study. The CTA membrane was composed of a cellulose triacetate layer with an embedded woven support mesh (Cath et al. 2006, McCutcheon and Elimelech 2008). The TFC membrane was made of a thin selective polyamide active layer on top of a porous polysulfone support layer (Cath et al. 2013, McGinnis et al. 2013). The CTA membrane surface was abundant with hydroxyl functional groups, while the TFC membrane surface was enriched by carboxylic functional group. Details regarding the membrane surface chemistry can be found in our previous publication (Xie and Gray 2016). A comprehensive membrane characterisations for both CTA and TFC membranes were provided in the Supplementary Data, including estimated pore size (Table S1), membrane surface zeta potential (Figure S3), membrane surface chemistry (Figure S3), membrane contact angle (Table S4), and surface roughness (Figure S4).

Silica stock solutions with a concentration of 0.2 M Na_2SiO_3 were prepared by dissolving sodium metasilicate ($Na_2SiO_3 \cdot 9H_2O$, assay>98%, Sigma-Aldrich) in MilliQ water. The stock solution was prepared freshly to avoid undesirable silica condensation (Felmy et al. 2001). The stock solution was dosed into a background electrolyte containing 20 mM NaCl and 1 mM $NaCHO_3$ at solution pH of 6.5. The reactive silica concentration of the working solution was determined by the molybdate yellow method (Method 8185, Hach DR5000) at wavelength of 815 nm.

2.2. FO setup and silica scaling experimental protocol

The FO membrane cell was made of acrylic plastic and designed to hold a flat-sheet membrane under moderate pressure differential without any physical support. Flow channels were engraved in acrylic blocks that made up the feed and permeate semi-cells. Each channel was 2 mm deep, 90 mm wide, and 120 mm long. Details of this FO filtration setup were provided in our previous publications (Xie and Gray 2016, Xie et al. 2016b), and can be found at Figure S1, Supplementary Data. Crossflow rate of 1 L/min (corresponding to crossflow velocity of 9 cm/s) was maintained for both the feed and draw solutions using micro gear pumps. The FO water flux was determined by measuring the weight changes of the feed solution at specific time intervals with a precision balance connected to a computer and a data logging system.

Silica scaling experiment was performed on both CTA and TFC membranes. The same initial water flux of 25 L m^{-2} h^{-1} was achieved for both the CTA and TFC membranes using NaCl draw solution (2.5 M for CTA membrane; and 1.5 M for TFC membrane). Specifically, a new membrane sample, with the active layer facing the feed solution, was placed in the membrane cell before each experiment and stabilised in FO mode with deionised water for one hour to obtain a stable water flux. Next, the silica scaling experiment was performed for about 24 h to obtain approximately 1,600 mL cumulative permeate volume at the conclusion of each experiment. The silica scaling solution contained a reactive silica concentration of 6 mM in a background electrolyte containing 20 mM NaCl and 1 mM $NaCHO_3$ at solution pH of 6.5, which resulted in a silica saturation index of 1.6. Other experimental conditions were: cross-flow rate of 1 L/min (corresponding to the cross-flow velocity of 9 cm/s), ambient pH (pH 6.5), and temperature of 25.0 ± 0.1°C. Water flux was continuously monitored throughout the fouling experiments by a data logger. A baseline experiment (i.e., feed without silica foulant) was also

carried out to correct the flux decline due to the continuous concentration of the feed solution and dilution of the draw solution, as described in our previous publication (Xie et al. 2015b). The feed solution was continuously sampled to quantify the evolution of silica polymerisation. At the conclusion of each scaling experiment, the scaled membrane was air dried in a desiccator for scanning electron microscopy imaging.

2.3. Quantification of silica polymerisation during scaling

Mass spectrometry and light scattering were used to continuously track the growth and polymerisation silica from reactive silica (including a range of low molecular weight monomers, dimers, and trimers), to colloidal silica. Combining these techniques allowed us to capture the entire silica polymerisation process, thereby facilitating the understanding of silica scaling mechanism.

Electrospray ionization mass spectrometry (ESI-MS) was used to identify the evolution of reactive silica species. The ESI-MS spectra were recorded by direct infusion in negative ion mode for 15 minutes. The feed liquid sample was diluted by methanol (50/50, v:v) to enhance electrospray ionization process and minimize ion suppression. The direct infusion flow of the analyte was 10 µL/min. ESI negative ionization was used with a detector voltage of 3 kV, desolvation temperature of 250 ºC, and heating block temperature of 200 ºC. High purity nitrogen was used as the nebulizing gas at a flowrate of 1 L/min. The time-average MS spectra were reported to identify the silica size and structure.

Dynamic and static light scattering were used to monitor the hydrodynamic radius of silica and weight-average molecular weight of silica. Light scattering experiments were conducted with a multi-angle goniometer setup (BI-200SM, Brookhaven Instruments, NY, USA) with a He−Ne laser with a wavelength of 633 nm as a light source. Dynamic light scattering

measurements were obtained with a fixed detector at 90°. For static light-scattering measurements, the normalized scattered light intensity was obtained by altering detector over an angular range of 17 – 135°, corresponding to wave vectors $0.0046 < q < 0.0305$ nm^{-1}. The scattering intensities from static light scattering obtained as Rayleigh ratios at an angle θ were processed in a Zimm plot in order to obtain the weight-averaged molar mass. The feed solution samples were monitored continuously over the scaling experiment to record the hydrodynamic radius and weight-averaged molar mass of silica.

2.4. Kinetics and characterisation of silica scaling in FO membrane

A series of silica scaling experiments with varying saturation index (i.e., initial reactive silica concentration) were conducted on both CTA and TFC membranes in order to elucidate the silica scaling mechanisms. Three silica saturation indexes were used, namely 0.8, 1.29 and 2.0. SEM-based imaging analysis was used to quantify the silica nucleation event on membrane surface. Silica scaling experiment was terminated once the static light scattering was able to detect the weight-average molecular molar mass: three-hour for TFC membrane, and five-hour for CTA membrane. Numbers of silica crystals on the SEM images were used to estimate the silica nucleation kinetic parameters for CTA and TFC membranes. Specifically, silica surface nucleation rate is given by (Tobler et al. 2009)

$$N_n = Aexp\left(-\frac{\Delta G^*}{k_B T}\right) \qquad (1)$$

where N_n, steady-state surface nucleation rate (number of nucleation events per square meter per second), ΔG^*, thermodynamic barrier to forming a silica crystal, $k_B T$, product of Boltzmann constant and system temperature, and A, kinetic constant, whose value depends upon many physical parameters including diffusional and steric barriers.

Using the classical nucleation theory (Wallace et al. 2009), ΔG^* can be expressed in terms of silica saturation index, σ:

$$\Delta G^* = B\left(\frac{k_B}{\delta}\right) \quad (2)$$

where B is a shape-specific constant, which was determined directly from experimental observations without direct knowledge or assumption of nucleus shape. Combining eqs 1 and 2 and then rewriting into linear form gives

$$lnN_n = lnA - B\left(\frac{1}{\sigma^2}\right) \quad (3)$$

where the slope, B, is directly proportional to the energy barrier to silica nucleation and the intercept, ln A, contains kinetic factors that govern nucleation frequency.

To provide further evidence in regard to the silica-membrane interaction during scaling, we also employed an X-ray photoelectron spectroscopy (XPS) to examine the interface between silica and membrane. Bond chemistry of silica scaled membrane surface layer was analysed by high resolution Si 2p scan. Specifically, XPS analysis used monochromatic aluminium Kα X-ray photoelectron spectrometer (Thermo Scientific, MA). A spot size of 400 μm^2 was used to scan in the region of the Si 2p binding energy at 20 eV pass energy. Two random spots on duplicate membrane samples were selected. Excessive charging of the samples was minimized using an electron flood gun. High resolution scans had a resolution of 0.1 eV. The high resolution XPS spectra were subtracted by the Shirley-type background, and Gaussian-Lorentz peak deconvolution was performed to estimate the binding energy shift of silicon Si 2p. The signal residual after deconvolution was also plotted to assure accuracy (Figure S2, Supplementary Data).

3. Results and Discussion

3.1. Silica scaling behaviour

Markedly different silica scaling profile was observed between CTA and TFC membranes in terms of water flux decline and silica scaling morphology (Figure 1). Generally, the CTA membrane exhibited more resilience against silica scaling in comparison with the TFC membrane. The CTA membrane demonstrated a gradual decrease in water flux during silica scaling (Figure 1A). However, unlike the CTA membrane, the TFC membrane was subjected to two distinct stages of water flux decline: water flux decreased significantly from 25 to 17 L m^{-2} h^{-1} during the first four hours of filtration (Figure 1A). The varying water flux decline profile also resulted in markedly different silica scaling morphology at the conclusion of the experiment (Figure 1B and C). Silica scaling morphology on the CTA membrane was sparsely distributed with clear crystal shape (Figure 1B), indicating the majority of silica was deposited on the membrane surface; by contrast, that on the TFC membrane was amorphous and compact (Figure 1C), and it was hypothesised that silica scaling was initiated by reactive silica nucleation on the TFC membrane surface, followed by continuous silica polymerisation during scaling. Previous studies also showed occurrence of silica polymerisation on the TFC membrane, resulting in silica gelation on membrane surface (Mi and Elimelech 2013). These observations suggested that silica scaling mechanisms on the CTA and TFC membranes were different, thereby warranting a close examination of silica scaling evolution.

[Figure 1]

3.2. Silica species characteristics during scaling

3.2.1. Mass spectra identified the evolution of reactive silica oligomers

Mass spectra provided critical information on the evolution of oligomers during reactive silica scaling. We compared time-resolved mass spectra of silica oligomers in the feed solution for both CTA and TFC membranes during the first ten-hour of filtration (Figure 2), and tabulated the mass/charge ratio (m/z) and possible structure of silica oligomers (Table 1). For both membranes, silica scaling was initiated via mono-silicic acid, which was evident by the m/z of 113 (Table 1) (Belton et al. 2012). However, the evolution routes of silica oligomers were significantly different between the CTA and TFC membrane. For the CTA membrane, the oligomerisation of monomer silica proceeded via formation of dimmer – linear trimer – cyclic trimer (Figure 2 A and Table 1) silicates (Bussian et al. 2000, Jiang and Wan 2015). This observation indicated that the deposition of silica on the CTA membrane is likely to occur via a homogeneous nucleation process, with silica aggregates formed in the bulk solution prior to deposition onto the membrane surface. This hypothesis was also consistent with the silica scaling morphology, as distinct silica crystals at the conclusion the scaling experiment were observed (Figure 1B). By contrast, silica polymerisation induced by the TFC membrane reached a plateau after six-hour filtration (Figure 2B), where the major species of silica oligomers in the solution remained as cyclic trimer as m/z of 398.9 (Table 1) after ten-hour scaling experiment (Eggers et al. 2005). It is hypothesized that mono-silicic acid was adsorbed on the membrane surface, thereby initiating silica polymerisation on the membrane surface and resulting in an amorphous silica scaling morphology at the conclusion of experiment (Figure 1C). It also agreed with the majority of mono-silicic acid being depleted from aqueous solution after 10 hours filtration, and the formation of varying structures of silica oligomers was limited. This quick consumption of reactive silica during TFC membrane scaling was also confirmed by a severe decrease of reactive silica concentration in comparison with the CTA membrane (Figure 3).

[Figure 2]

[Table 1]

[Figure 3]

3.2.2. Dynamic and static light scattering profiled the growth and structure of reactive silica

In order to provide further evidence of the varying silica scaling mechanisms during CTA and TFC membrane filtration, dynamic and static light scattering was also employed to capture the silica aggregate profiles. Dynamic light scattering continuously monitored the hydrodynamic radii of silica in the scaling experiment (Figure 4). As expected, we observed a gradual increase in silica hydrodynamic radii from 12 to 25 nm by the CTA membrane. By contrast, despite a slight increase in the silica hydrodynamic radii in the first four-hours of filtration by TFC membrane, the silica hydrodynamic radii largely remained unchanged. This observation agreed well with the trend of mass spectra reported in the previous section (section 3.2.1). In addition, static light scattering together with a Zimm plot revealed the estimated weight-average molecular weight present during scaling (Figure 4). For TFC membrane, the weight-average molecular weight of silica increased swiftly and reached plateau after six hours, which was consistent with the mass spectra as well as the hydrodynamic radii detected by dynamic light scattering. However, for the CTA membrane, the weight-average molecular weight increased gradually, which was in line with the mass spectrometry data.

[Figure 4]

Both increase in hydrodynamic radii as well as the weight-average molecular weight suggested that the mechanism of silica scaling for the CTA membrane was driven by the aggregation of mono-silicic acid and resulted in the growth of relatively large silica aggregates in

the bulk solution. On the other hand, the faster consumption of mono-silicic acid, and relatively stable hydrodynamic radii and weight-average molecular weight during the TFC membrane scaling indicated that the majority of mono-silicic acid interacted with the membrane surface, thereby facilitating the surface silica polymerisation. The evidence from light scattering as well as analysis of mass spectra supported this hypothesis.

3.3. Silica scaling mechanisms

3.3.1. Thermodynamic parameters of silica surface nucleation

The thorough analysis of the aqueous solution with varying techniques suggested the different silica scaling mechanisms for the CTA and TFC membrane. We herein explored the silica-membrane surface interaction during scaling to provide further support for the hypotheses. A set of scaling experiments with varying silica saturation indexes were conducted to extract key thermodynamic and kinetic parameters for silica scaling during CTA and TFC membrane filtration using Equation 3. Silica scaling experiment was terminated once static light scattering was able to detect the weight-average molecular molar mass for silica species in the feed to either CTA or TFC membranes. The number of SEM identifiable crystals per specific membrane surface area was assumed to be initiated by one nucleation event, N_n. As expected, the CTA membrane was resilient to silica scaling, which was evident by largely unchanged nucleation events under three saturation indexes (upper row, Figure 5). By contrast, a clear increase of silica crystals was observed on the TFC membrane surface with an increase of saturation indexes (lower row, Figure 5). These results further corroborated the observation of silica species in the aqueous solution, indicating different scaling mechanisms.

By plotting and linear fitting nucleation events as a function of solution saturation state (Figure 6), we estimated the energy barrier to silica nucleation, B; and nucleation frequency, A,

based on the Equation 3. The estimated silica nucleation energy barrier, B was 5.89 ± 1.21, and 2.28 ± 0.88, for CTA and TFC membranes, respectively; while the nucleation frequency, lnA, were 16.9 ± 3.2, and 19.6 ± 4.3, for CTA and TFC membranes, respectively. These parameters demonstrated a significant reduction of surface nucleation energy (more than 50%) for the TFC membrane in comparison with the CTA. Surface nucleation is driven primarily by interfacial energy, which manifests itself as reductions in the thermodynamic barrier to crystal formation specifically at the solution-membrane interface. The ability of a given membrane surface to facilitate surface nucleation is largely attributed to the magnitude of the free energy reduction. Indeed, such decrease in the surface nucleation on the TFC membrane substantially promoted silica surface polymerisation, where the majority of mono-silicic acids interacted with the TFC membrane surface to initiate silica polymerisation. In addition, the silica surface nucleation energy barrier, ΔG^*, resulted from its dependence upon the liquid-membrane interfacial energy. A previous study reported that the CTA membrane possessed a higher liquid-membrane interfacial energy (37.1 mJ/m^2) than the TFC membrane (34.1 mJ/m^2) estimated from contact angle measurements (Coday et al. 2015, Coday et al. 2016). As a result, the TFC membrane surface was more favourable to silica surface polymerisation in comparison with the CTA membrane.

Via estimating key thermodynamic parameters, we confirmed that the mechanism of silica scaling on the TFC membrane was mainly driven by the silica surface polymerisation; while that on the CTA membrane was due to the silica aggregation in the bulk solution and subsequent deposition onto the membrane surface. However, the chemical origin of such different silica-membrane surface interaction remained unknown. By an indirect force measurement by atomic force microscopy, previous study suggested that the difference in silica

scaling between CTA and TFC membrane was due to the varied capabilities in forming hydrogen bonding (Mi and Elimelech 2013). However, in the case of carboxylic functional group, its O-H group is even more strongly polarized than the hydroxyl functional group due to the presence of the adjacent carbonyl moiety. Presence of such dipoles in carboxylic functional group allows participation in energetically favourable hydrogen bonding interactions (Brück et al. 2000), functioning as both a hydrogen bond donor and acceptor. As a result, exploring the chemical origin of varying silica scaling profiles between CTA and TFC membranes remains critical to understand the silica scaling mechanisms.

[Figure 5]

[Figure 6]

3.3.2. Chemical origin of silica-membrane interaction

High resolution XPS was used to examine the chemical state of Si 2p at the conclusion of silica scaling by the CTA and TFC membranes in order to elucidate the chemical origin of silica-membrane surface interaction between CTA and TFC membrane.

Marked differences were present in the binding energy of Si 2p for the CTA and TFC membranes at the conclusion of the experiment (Figure 7). Specifically, for the CTA membrane, the peak of Si 2p binding energy was 105.2 eV, which was the characteristic bond of Si = O (Bashouti et al. 2012, Yan et al. 2013). By contrast, for the TFC membrane, the Si 2p binding energy peak was 103.8 eV, which corresponded to the Si-O bond (Kim et al. 2015, Niu et al. 2015). The varying Si 2p binding energy profile shed light on the different silica scaling mechanisms of CTA and TFC membranes. Indeed, for CTA membrane, the majority of scalants were composed of silica aggregates, which were deposited onto the membrane surface after

aggregation of mono-silicic acid the subsequent growth in the liquid phase. As a result, the Si = O bond with Si 2p binding energy of 105.2 eV originated from the relatively large silica aggregates, without strong interaction with membrane surface. However, on the other hand, the TFC membrane possessing carboxylic functional group with stronger hydrogen bonding capacity enabled significant silica surface polymerisation, where the major Si 2p binding energy was 103.8 eV as Si-O bond. This TFC membrane surface interacted with mono-silicic acid via adsorption, with a relatively low surface nucleation energy barrier (Section 3.3.1), the mono-silicic acid formed Si-O bond with abundant carboxylic functional groups on the TFC membrane surface. As a result, silica surface polymerisation was the dominant mechanism for silica scaling of TFC membrane.

Based on the aforementioned results, it was plausible to picture silica scaling mechanisms from solution to membrane interface during FO filtration by the CTA and TFC membranes (Figure 8). For the CTA membrane, due to the relatively higher surface nucleation energy barrier and lower silica-membrane interaction, the majority of monosilicic acid was aggregated in the aqueous solution, which was evident by both mass spectra and light scattering measurements. The silica aggregates then deposited onto the membrane surface, resulted in a sparse silica scaling morphology as well as a strong signal of Si=O bond characteristic of silica aggregates. However, the silica scaling was manifested in a different mechanism by the TFC membrane. Monosilicic acid preferred to interact with TFC membrane surface where a lower surface nucleation energy barrier and a stronger silica-membrane affinition were presented. As a result, the silica aggregation in the aqueous phase was not severe. Rather the strong signal for Si-O binding energy was shown on the TFC membrane surface, which strongly supports the silica surface polymerisation mechanism.

[Figure 7]

3.3.3. Implications

Varying silica scaling mechanisms reported here has implication in tuning membrane surface chemistry with anti-scaling property for treating challenging waste streams, such as seawater brine and brackish groundwater, both of which are heavily laden with silica. Insights from this study also provide means for better understanding silica behaviour in the aqueous solution as well as during interaction with different membrane surfaces. In addition, evidence for different silica scaling mechanisms also suggests a plausible explanation for the role of membrane surface in silica scaling.

Based on the experimental results and corresponding silica scaling mechanisms, two major strategies can be proposed. First, membrane surface chemistry should be carefully tuned during interfacial polymerisation, such as using monomer with less acyl chloride groups, thereby reducing surface carboxyl group density of polyamide layer. On the other hand, reducing oligomers for reactive silica aggregation can significantly minimize silica scaling. Thus, from an operation perspective, simple but effective pre-treatment of feed streams can enhance membrane performance.

4. Conclusion

Results reported here suggested that silica scaling mechanisms on the CTA and TFC membranes were largely different. For CTA membrane, silica scaling was promoted by the aggregation of mono-silicic acid into large silica aggregates, followed by the deposition from bulk solution onto the membrane surface; by contrast, silica surface polymerisation on the TFC

membrane was the dominant mechanism where the majority of mono-silicic acid interacted with TFC membrane surface, which was followed by polymerisation of silica on the membrane surface resulting in severe water flux reduction. This hypothesis was supported by monitoring of aqueous silica species with mass spectrometry and light scattering techniques; as well as confirmed by the estimation of key silica nucleation parameters and high-resolution XPS analysis of Si 2p binding energy on the CTA and TFC membrane. For the CTA membrane, the aggregation of monomer silicic acid proceed via formation of dimmer – linear trimer – cyclic trimer, which resulted in a continuous increase in hydrodynamic radii as well as the weight-average molecular weight. However, for the TFC membrane, the major species of silica oligomers in the solution remained as cyclic trimer after ten-hours of scaling experiment, which was compounded by a largely unchanged hydrodynamic radii and weight-average molecular weight. Estimation of thermodynamic parameters of silica surface nucleation demonstrated a significant reduction of surface nucleation energy (more than 50%) for the TFC membrane in comparison with the CTA. In addition, the Si 2p binding energy suggested different silicon bonds for the CTA (Si=O) and TFC (Si-O) membranes, which supported the proposed chemical origins of silica scaling on these two membranes.

5. Acknowledgements

M.X. thanked Victoria University for the award of Vice Chancellor Early Career Fellowship. Dr. Yichao Wang (Royal Melbourne Institute of Technology) was thanked for the discussion and technical assistance in XPS analysis.

6. References

Achilli, A., Cath, T.Y., Marchand, E.A. and Childress, A.E. (2009) The forward osmosis membrane bioreactor: A low fouling alternative to MBR processes. Desalination 239(1–3), 10-21.

Bashouti, M.Y., Sardashti, K., Ristein, J. and Christiansen, S.H. (2012) Early stages of oxide growth in H-terminated silicon nanowires: determination of kinetic behavior and activation energy. Physical Chemistry Chemical Physics 14(34), 11877-11881.

Belton, D.J., Deschaume, O. and Perry, C.C. (2012) An overview of the fundamentals of the chemistry of silica with relevance to biosilicification and technological advances. FEBS Journal 279(10), 1710-1720.

Boo, C., Lee, S., Elimelech, M., Meng, Z. and Hong, S. (2012) Colloidal fouling in forward osmosis: Role of reverse salt diffusion. Journal of Membrane Science 390–391(0), 277-284.

Brück, A., McCoy, L.L. and Kilway, K.V. (2000) Hydrogen Bonds in Carboxylic Acid−Carboxylate Systems in Solution. 1. In Anhydrous, Aprotic Media. Organic Letters 2(14), 2007-2009.

Bussian, P., Sobott, F., Brutschy, B., Schrader, W. and Schüth, F. (2000) Speciation in Solution: Silicate Oligomers in Aqueous Solutions Detected by Mass Spectrometry. Angewandte Chemie International Edition 39(21), 3901-3905.

Cath, T.Y., Gormly, S., Beaudry, E.G., Flynn, M.T., Adams, V.D. and Childress, A.E. (2005) Membrane contactor processes for wastewater reclamation in space: Part I. Direct osmotic concentration as pretreatment for reverse osmosis. Journal of Membrane Science 257(1-2), 85-98.

Cath, T.Y., Childress, A.E. and Elimelech, M. (2006) Forward osmosis: Principles, applications, and recent developments. Journal of Membrane Science 281(1-2), 70-87.

Cath, T.Y., Elimelech, M., McCutcheon, J.R., McGinnis, R.L., Achilli, A., Anastasio, D., Brady, A.R., Childress, A.E., Farr, I.V., Hancock, N.T., Lampi, J., Nghiem, L.D., Xie, M. and Yip, N.Y. (2013) Standard Methodology for Evaluating Membrane Performance in Osmotically Driven Membrane Processes. Desalination 312(0), 31-38.

Coday, B.D., Almaraz, N. and Cath, T.Y. (2015) Forward osmosis desalination of oil and gas wastewater: Impacts of membrane selection and operating conditions on process performance. Journal of Membrane Science 488, 40-55.

Coday, B.D., Hoppe-Jones, C., Wandera, D., Shethji, J., Herron, J., Lampi, K., Snyder, S.A. and Cath, T.Y. (2016) Evaluation of the transport parameters and physiochemical properties of forward osmosis membranes after treatment of produced water. Journal of Membrane Science 499, 491-502.

Cornelissen, E.R., Harmsen, D., de Korte, K.F., Ruiken, C.J., Qin, J.-J., Oo, H. and Wessels, L.P. (2008) Membrane fouling and process performance of forward osmosis membranes on activated sludge. Journal of Membrane Science 319(1-2), 158-168.

Eggers, K., Eichner, T. and Woenckhaus, J. (2005) Mass spectrometric investigation of small silicate polyhedra in solution. International Journal of Mass Spectrometry 244(1), 72-75.

Elimelech, M. and Phillip, W.A. (2011) The Future of Seawater Desalination: Energy, Technology, and the Environment. Science 333(6043), 712-717.

Felmy, A.R., Cho, H., Rustad, J.R. and Mason, M.J. (2001) An Aqueous Thermodynamic Model for Polymerized Silica Species to High Ionic Strength. Journal of Solution Chemistry 30(6), 509-525.

Holloway, R.W., Childress, A.E., Dennett, K.E. and Cath, T.Y. (2007) Forward osmosis for concentration of anaerobic digester centrate. Water Research 41(17), 4005-4014.

Jiang, Y. and Wan, Q.-H. (2015) Separation and identification of oligomeric phenylethoxysiloxanols by liquid chromatography-electrospray ionization mass spectrometry. Journal of Chromatography A 1394, 95-102.

Kim, K.H., Lee, D.J., Cho, K.M., Kim, S.J., Park, J.-K. and Jung, H.-T. (2015) Complete magnesiothermic reduction reaction of vertically aligned mesoporous silica channels to form pure silicon nanoparticles. Scientific Reports 5, 9014.

Lee, S., Boo, C., Elimelech, M. and Hong, S. (2010) Comparison of fouling behavior in forward osmosis (FO) and reverse osmosis (RO). Journal of Membrane Science 365(1–2), 34-39.

Li, Z.-Y., Yangali-Quintanilla, V., Valladares-Linares, R., Li, Q., Zhan, T. and Amy, G. (2012) Flux patterns and membrane fouling propensity during desalination of seawater by forward osmosis. Water Research 46(1), 195-204.

McCutcheon, J.R. and Elimelech, M. (2008) Influence of membrane support layer hydrophobicity on water flux in osmotically driven membrane processes. Journal of Membrane Science 318(1-2), 458-466.

McGinnis, R.L., Hancock, N.T., Nowosielski-Slepowron, M.S. and McGurgan, G.D. (2013) Pilot demonstration of the NH3/CO2 forward osmosis desalination process on high salinity brines. Desalination 312(0), 67-74.

Mi, B. and Elimelech, M. (2010) Organic fouling of forward osmosis membranes: Fouling reversibility and cleaning without chemical reagents. Journal of Membrane Science 348(1-2), 337-345.

Mi, B. and Elimelech, M. (2013) Silica scaling and scaling reversibility in forward osmosis. Desalination 312, 75-81.

Milne, N.A., O'Reilly, T., Sanciolo, P., Ostarcevic, E., Beighton, M., Taylor, K., Mullett, M., Tarquin, A.J. and Gray, S.R. (2014) Chemistry of silica scale mitigation for RO desalination with particular reference to remote operations. Water Research 65, 107-133.

Niu, J., Zhang, S., Niu, Y., Song, H., Chen, X., Zhou, J. and Cao, B. (2015) Direct amination of Si nanoparticles for the preparation of Si@ultrathin SiOx@graphene nanosheets as high performance lithium-ion battery anodes. Journal of Materials Chemistry A 3(39), 19892-19900.

Shaffer, D.L., Werber, J.R., Jaramillo, H., Lin, S. and Elimelech, M. (2015) Forward osmosis: Where are we now? Desalination 356, 271-284.

Shannon, M.A., Bohn, P.W., Elimelech, M., Georgiadis, J.G., Marinas, B.J. and Mayes, A.M. (2008) Science and technology for water purification in the coming decades. Nature 452(7185), 301-310.

Tobler, D.J., Shaw, S. and Benning, L.G. (2009) Quantification of initial steps of nucleation and growth of silica nanoparticles: An in-situ SAXS and DLS study. Geochimica et Cosmochimica Acta 73(18), 5377-5393.

Valladares Linares, R., Yangali-Quintanilla, V., Li, Z. and Amy, G. (2011) Rejection of micropollutants by clean and fouled forward osmosis membrane. Water Research 45(20), 6737-6744.

Wallace, A.F., DeYoreo, J.J. and Dove, P.M. (2009) Kinetics of Silica Nucleation on Carboxyl- and Amine-Terminated Surfaces: Insights for Biomineralization. Journal of the American Chemical Society 131(14), 5244-5250.

Xie, M., Nghiem, L.D., Price, W.E. and Elimelech, M. (2013) A Forward Osmosis–Membrane Distillation Hybrid Process for Direct Sewer Mining: System Performance and Limitations. Environmental Science & Technology 47(23), 13486-13493.

Xie, M., Nghiem, L.D., Price, W.E. and Elimelech, M. (2014) Toward Resource Recovery from Wastewater: Extraction of Phosphorus from Digested Sludge Using a Hybrid Forward Osmosis–Membrane Distillation Process. Environmental Science & Technology Letters 1(2), 191-195.

Xie, M., Bar-Zeev, E., Hashmi, S.M., Nghiem, L.D. and Elimelech, M. (2015a) Role of Reverse Divalent Cation Diffusion in Forward Osmosis Biofouling. Environmental Science & Technology 49(22), 13222-13229.

Xie, M., Lee, J., Nghiem, L.D. and Elimelech, M. (2015b) Role of pressure in organic fouling in forward osmosis and reverse osmosis. Journal of Membrane Science 493, 748-754.

Xie, M. and Gray, S.R. (2016) Gypsum scaling in forward osmosis: Role of membrane surface chemistry. Journal of Membrane Science 513, 250-259.

Xie, M., Shon, H.K., Gray, S.R. and Elimelech, M. (2016a) Membrane-based processes for wastewater nutrient recovery: Technology, challenges, and future direction. Water Research 89, 210-221.

Xie, M., Tang, C.Y. and Gray, S.R. (2016b) Spacer-induced forward osmosis membrane integrity loss during gypsum scaling. Desalination 392, 85-90.

Yan, N., Wang, F., Zhong, H., Li, Y., Wang, Y., Hu, L. and Chen, Q. (2013) Hollow Porous SiO2 Nanocubes Towards High-performance Anodes for Lithium-ion Batteries. Scientific Reports 3, 1568.

Zou, S., Gu, Y., Xiao, D. and Tang, C.Y. (2011) The role of physical and chemical parameters on forward osmosis membrane fouling during algae separation. Journal of Membrane Science 366(1–2), 356-362.

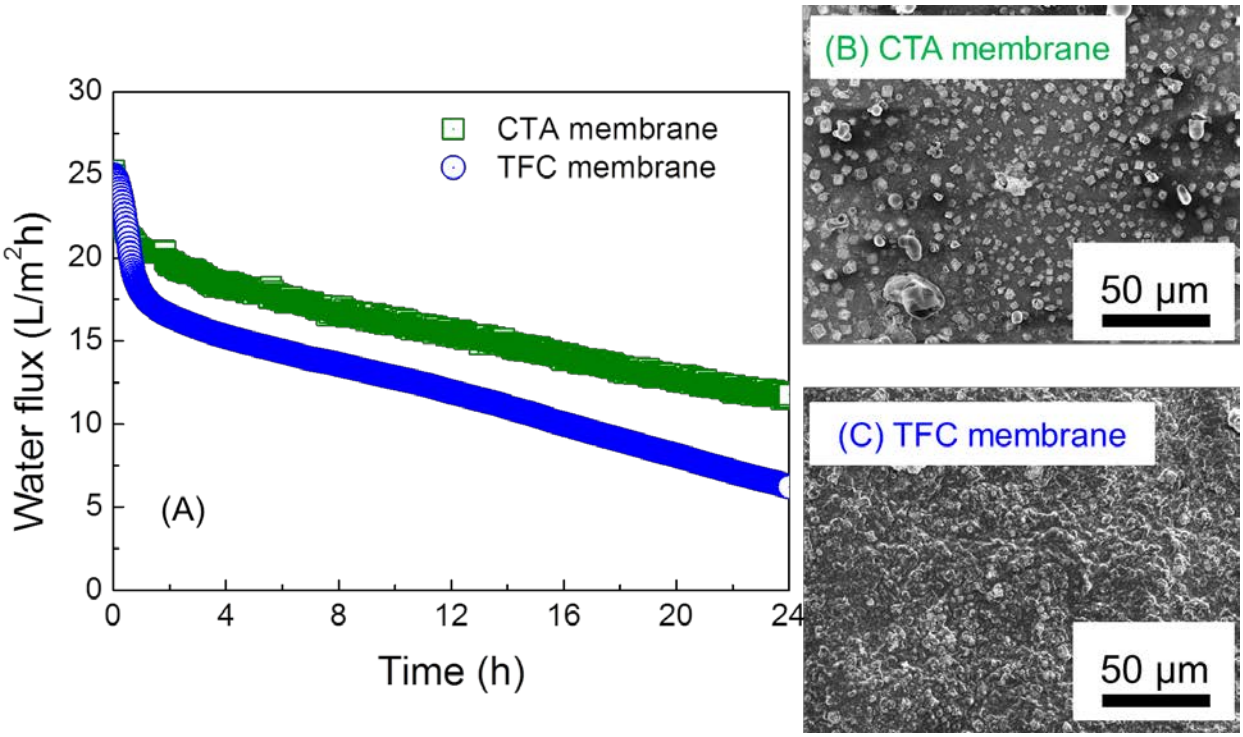

Figure 1: Silica scaling filtration by CTA and TFC membranes. (A) water flux decline by CTA and TFC membranes; representative micrographs of silica scaling morphology for (B) CTA membrane and (C) TFC membrane at the conclusion of the filtration. Experimental conditions were: The silica scaling solution contained a reactive silica concentration of 6 mM in a background electrolyte containing 20 mM NaCl and 1 mM $NaCHO_3$ at solution pH of 6.5. The NaCl draw solution concentrations were 2.5 and 1.5 M for CTA and TFC membranes, respectively. Operating conditions were: cross-flow rate of 1 L/min (corresponding to the cross-flow velocity of 9 cm/s), ambient pH (pH 6.5), and temperature of 25.0 ± 0.1°C. The filtration was operated for 24 hours, attaining 1,600 mL permeate.

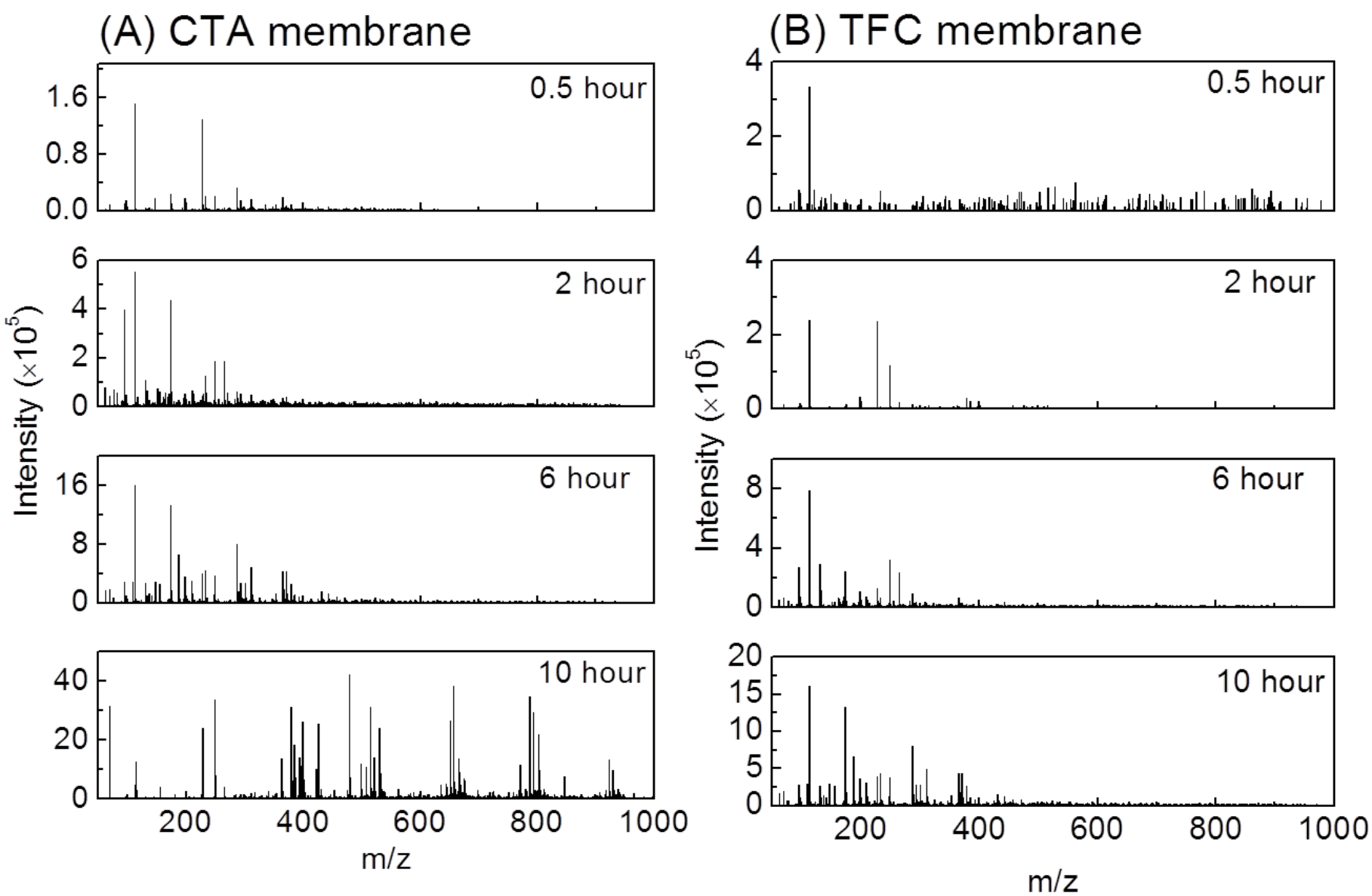
(A) CTA membrane
(B) TFC membrane
0.5 hour
2 hour
6 hour
10 hour
Intensity (×10^5)
m/z
200
400
600
800
1000

518

Figure 2: Mass spectra for (A) CTA and (B) TFC membranes during silica scaling. The feed solution was sampled at the specific time interval and was diluted with methanol. The mass spectrometry conditions were: The direct infusion flow of the analyte was 10 µL/min. Electrospray negative ionization was used with the detector voltage of 3 kV, desolvation temperature of 250 ºC, and heating block temperature of 200 ºC. High purity nitrogen was used as the nebulizing gas at a flowrate of 1 L/min.

Table 1: Possible structures of silica oligomers determined by electrospray ionization mass spectrometry during silica scaling. The possible structures of silica oligomers were estimated based on the m/z ratio, as well as silica chemistry in the literatures (Bussian et al. 2000, Eggers et al. 2005).

m/z identified	Possible molecular formula	Possible structure
113.0	$H_4SiO_4 \cdot H_2O$	
172.9	$H_5Si_2O_7$	
233.3	$H_5Si_3O_9$	
293.0	$H_5Si_4O_{11}$	
370.9	$H_7Si_5O_{14}$	
398.9	$H_6Si_6O_{14}$	
507.9	$H_{11}Si_8O_{17}$	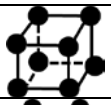
610.9	$H_{22}Si_9O_{28}$	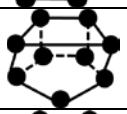
656.9	$H_{22}Si_{10}O_{29}$	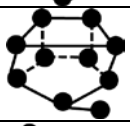
828.9	$H_{26}Si_{12}O_{28} \cdot H_2O$	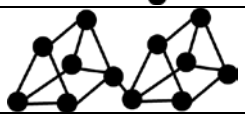

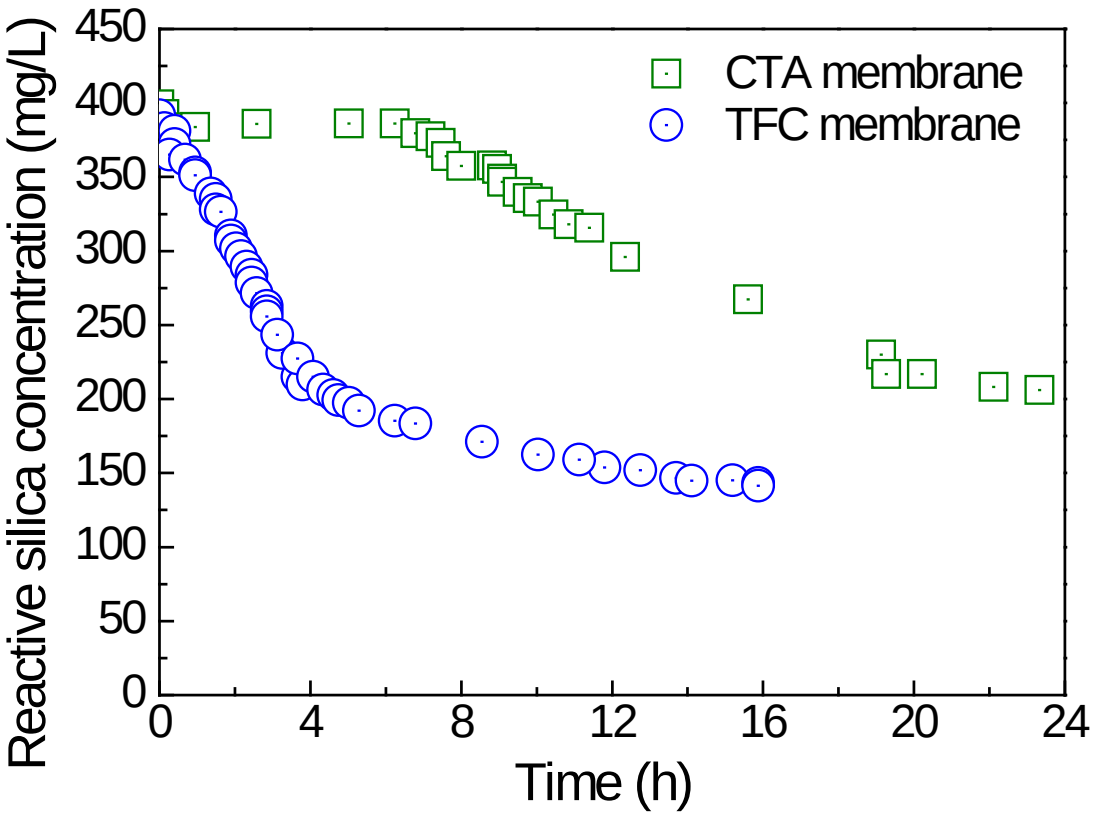

Figure 3: Reactive silica concentration as a function of filtration time for CTA and TFC membranes. The experimental conditions were described in Figure 1. The reactive silica concentration was determined by the molybdate yellow method (Method 8185, Hach DR5000) at wavelength of 815 nm.

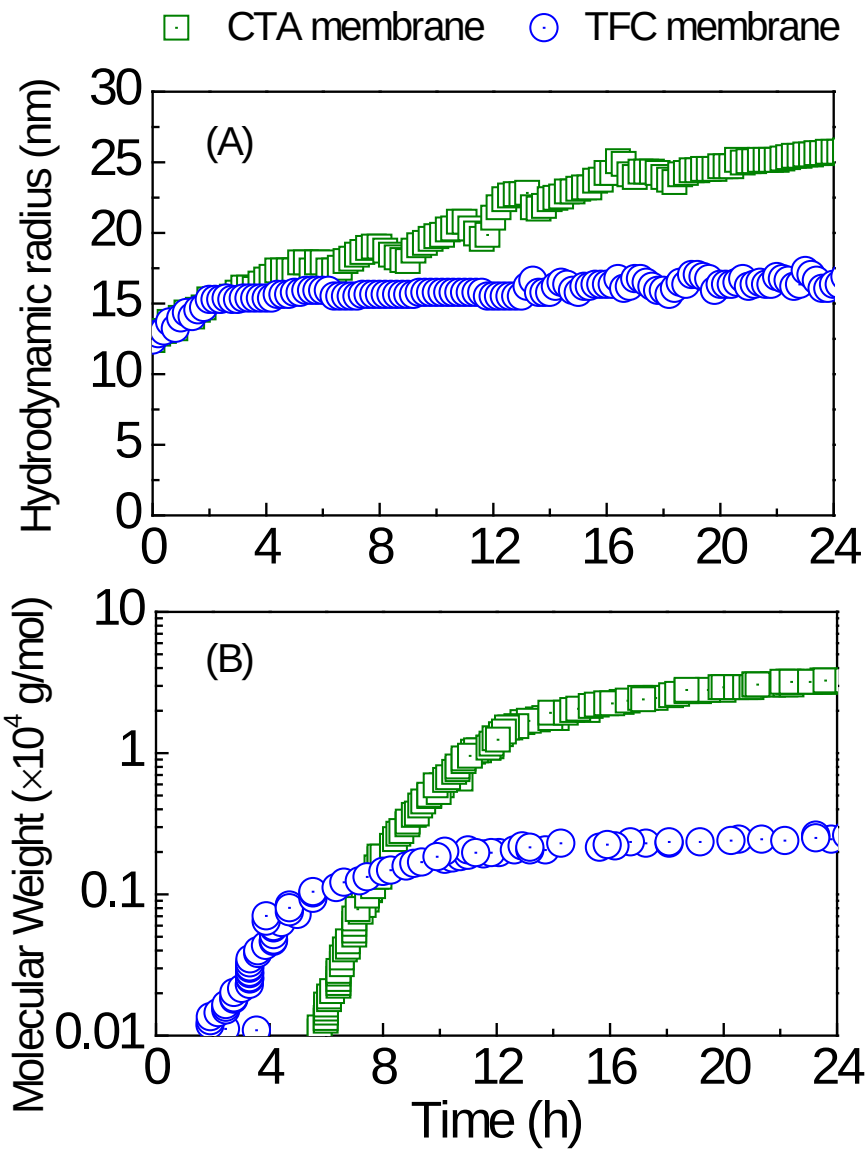

Figure 4: (A) Hydrodynamic radii and (B) weight-average molecular weights of silica feed solution during FO filtration by CTA and TFC membranes as a function of time. The experimental conditions were described in Figure 1. The hydrodynamic radii were determined by dynamic light scattering; while the weight-average molecular weight was estimated by static light scattering with Zimm plot.

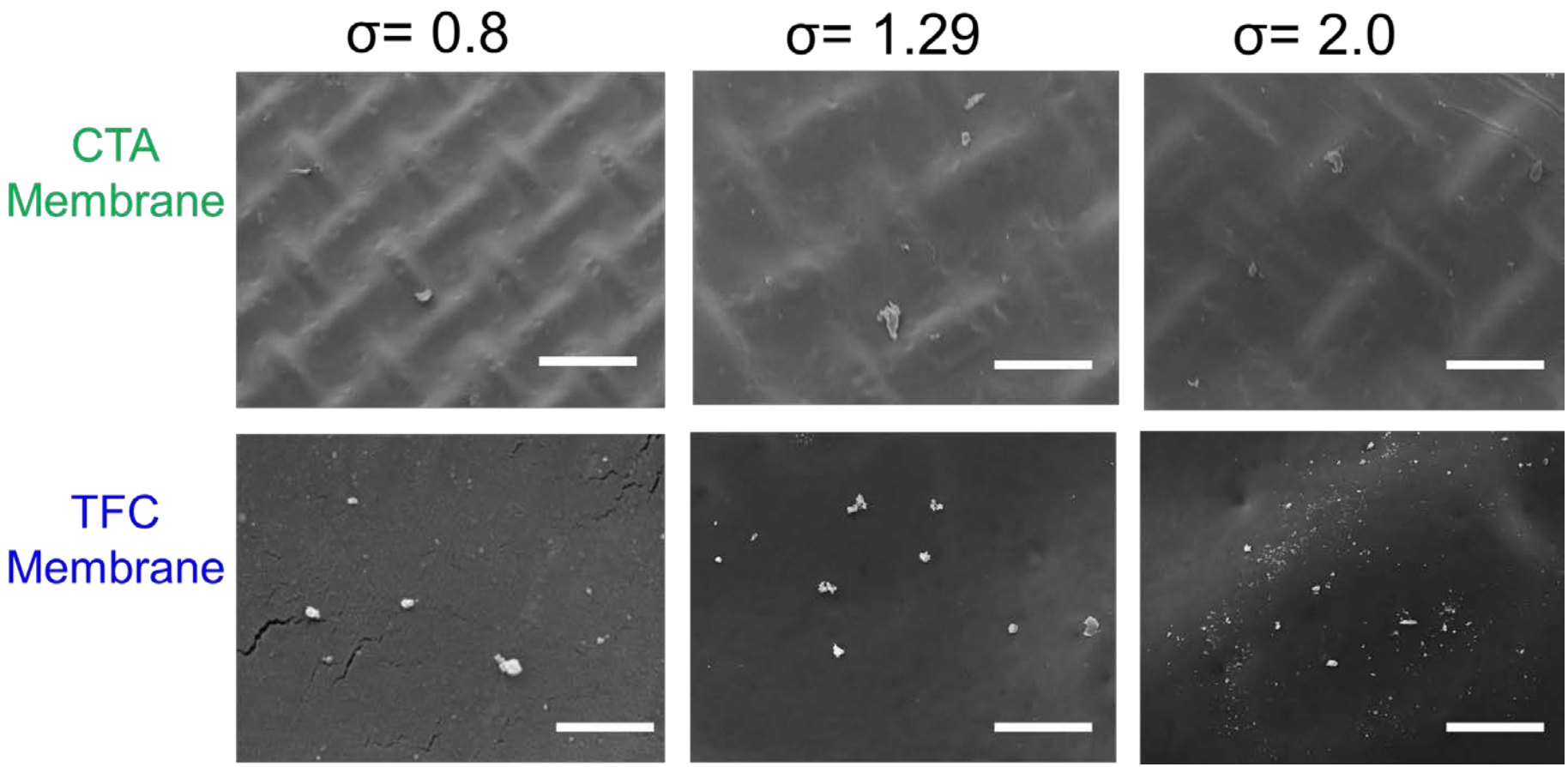

Figure 5: Representative micrographs of CTA (upper row) and TFC (lower row) membranes captured by scanning electron microscopy (SEM) at varying silica saturation indexes. The filtration experiment was terminated once the static light scattering was able to detect the weight-average molecular molar mass in the aqueous solution. The crystals identified by the SEM images were used to estimate silica surface nucleation parameters (showed in Figure 6). The bar in the SEM micrographs corresponds to 1 µm.

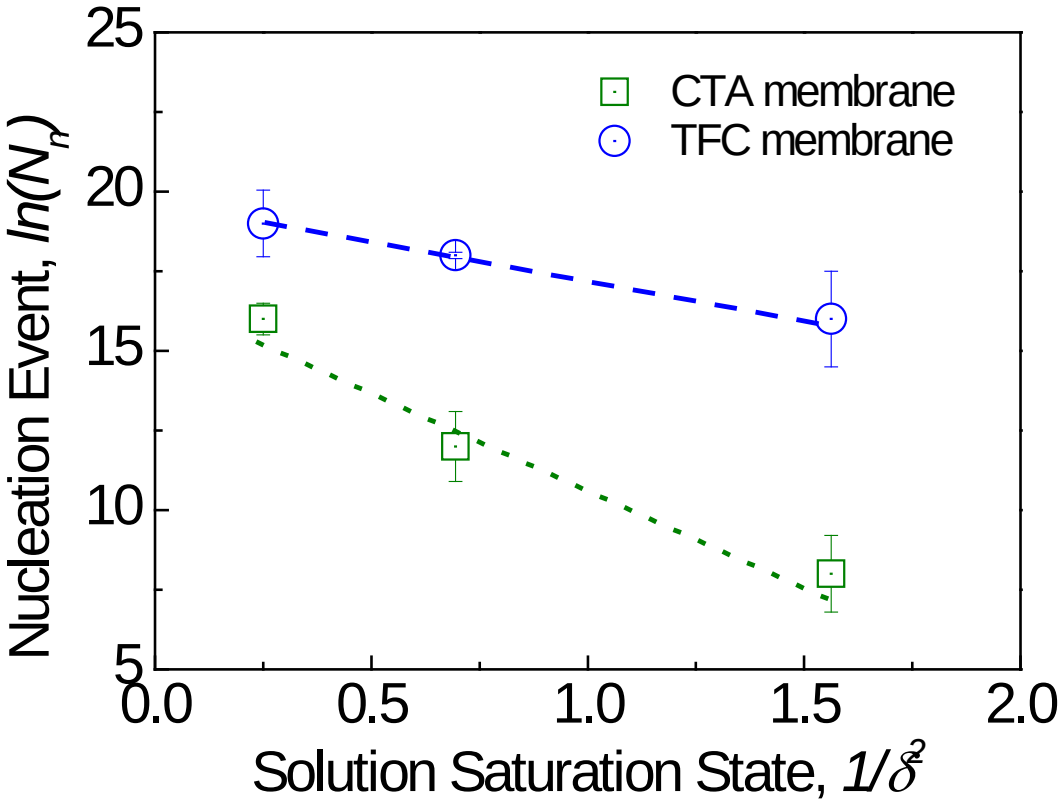

Figure 6: Estimation of silica surface nuleation parameters on CTA and TFC membranes by plotting the nucleation events (SEM-identifiable crystal number) as a function of the inverse square of saturation index. The experimental conditions were described in Figure 1. The slope of the trend line yields *B*, which is directly proportional to the energy barrier of nucleus formation ΔG^*.

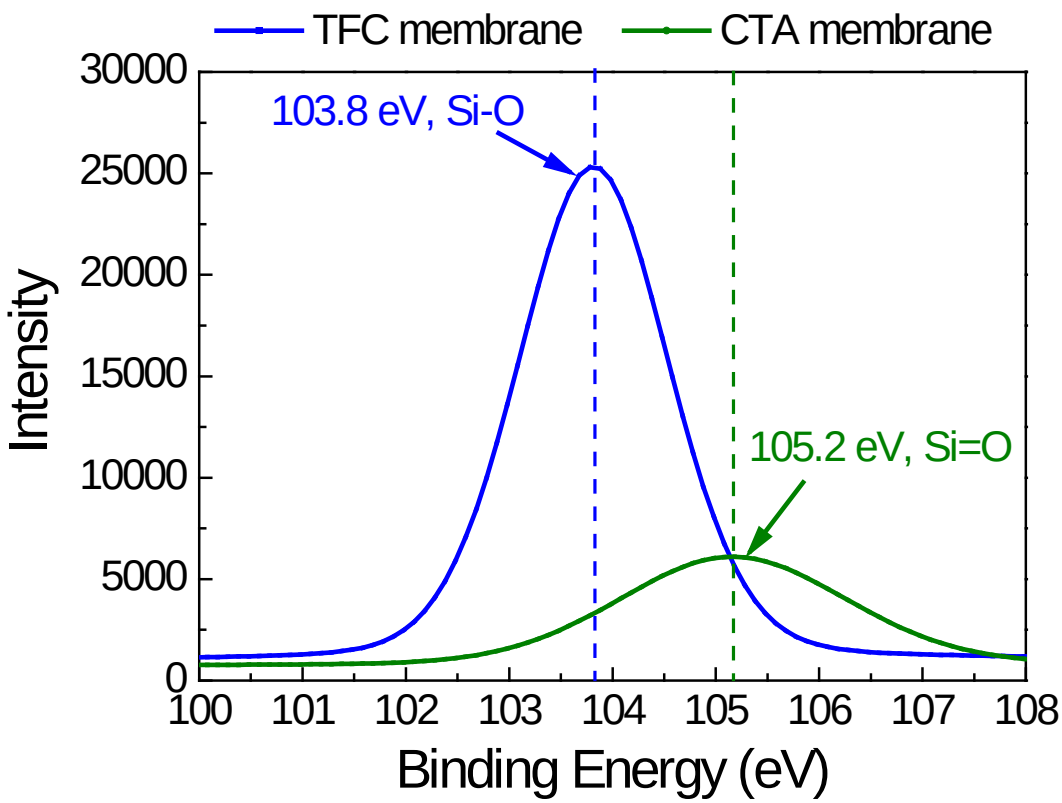

Figure 7: High resolution Si 2p scan by X-ray photoelectron spectroscopy of CTA and TFC membranes at the conclusion of silica scaling. Binding energy of Si 2p of 103.8 and 105.2 eV was for Si-O and Si=O bond, respectively.